JOC Article

Fast and Stable Photochromic Oxazines

Massimiliano Tomasulo,[†] Salvatore Sortino,*[,‡] Andrew J. P. White,[§] and Françisco M. Raymo*[,†]

Center for Supramolecular Science, Department of Chemistry, University of Miami, 1301 Memorial Drive, Florida, 33146-0431, Dipartimento di Scienze Chimiche, Universitá di Catania, viale Andrea Doria 8, Catania, I-95125, Italy, and Department of Chemistry, Imperial College London, South Kensington, London, SW7 2AY, U.K.

ssortino@unict.it; fraymo@miami.edu

Received July 8, 2005

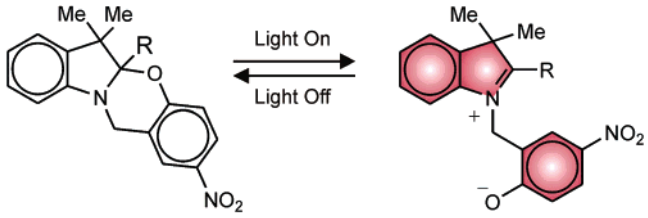

We have designed and synthesized two photochromic compounds incorporating fused indoline and benzooxazine fragments. Variable-temperature ^{1}H NMR spectroscopy demonstrates that their central [1,3]oxazine ring opens thermally with free energy barriers ranging from 14 to 19 kcal mol^{-1}. The ring-opened species reverts rapidly to the original isomer and can only be detected after chemical trapping. Specifically, the nucleophilic attack of a hydroxide anion to the indolium cation of the ring-opened species prevents re-isomerization. Laser excitation of both compounds induces the opening of the [1,3]oxazine ring in less than 6 ns with quantum yields up to 0.1. The photoinduced ring opening generates a 4-nitrophenolate chromophore, which absorbs strongly at 440 nm. The photogenerated species reverts to the original form with a lifetime of 22 ns for both compounds. Thus, these transformations can be exploited to interconvert the two isomers of each species with nanosecond switching speeds. Furthermore, thousands of switching cycles can be repeated consecutively without any sign of degradation, even in the presence of molecular oxygen. These processes can be reproduced efficiently in poly(methyl methacrylate) matrixes. Under these conditions, the thermal re-isomerization occurs with biexponential kinetics in submillisecond time scales. In principle, the fast isomerization kinetics and excellent fatigue resistance of both compounds offer the opportunity to modulate rapidly and efficiently a variety of molecular and macroscopic properties. Thus, our molecular design can evolve into the realization of a new family of photochromic compounds and materials with promising photoresponsive character.

Introduction

Spiropyrans combine two heterocyclic fragments in their molecular skeleton.[1−5] Often, one of them is a benzopyran with a nitro group in position 6, and the other is an indoline with two methyl groups in position 3. A common carbon atom with tetrahedral geometry connects the two fragments, forcing their mean planes in an orthogonal arrangement. The resulting molecules (e.g., **SP** in Figure 1) are colorless, but switch to colored merocyanines (e.g., **ME** in Figure 1) upon ultraviolet irradiation. In addition to imposing drastic absorbance changes in the visible region, the pronounced structural modifications associated with these photoinduced trans-

[†] University of Miami.
[‡] Universitá di Catania.
[§] Imperial College, London.

(1) (a) Bertelson, R. C. In *Photochromism*; Brown, G. H., Ed.; Wiley: New York, 1971; pp 45−431. (b) Bertelson, R. C. In *Organic Photochromic and Thermochromic Compounds*; Crano, J. C., Guglielmetti, R., Eds.; Plenum Press: New York, 1999; Vol. 1, pp 11−83.
(2) Kholmanskii, A. S.; Dyumanev, K. M. *Russ. Chem. Rev.* **1987**, *56*, 136−151.
(3) Guglielmetti, R. In *Photochromism: Molecules and Systems*; Dürr, H., Bouas-Laurent, H., Eds.; Elsevier: Amsterdam, 1990; pp 314−466 and 855−878.
(4) Tamai, N.; Miyasaka, H. *Chem. Rev.* **2000**, *100*, 1875−1890.
(5) Minkin, V. I. *Chem. Rev.* **2004**, *104*, 2751−2776.
(6) (a) Ichimura, K. In *Photochromism: Molecules and Systems*; Dürr, H., Bouas-Laurent, H., Eds.; Elsevier: Amsterdam, 1990; pp 903−918. (b) Ichimura, K.; Seki, T.; Kawamishi, Y.; Suzuki, Y.; Sakuragi, M.; Tamaki, T. In *Photo-Refractive Materials for Ultrathin Density Optical Memory*; Irie, M., Ed.; Elsevier: Amsterdam, 1994; pp 55−83. (c) Ichimura, K. In *Photochromic Polymers*; Crano, J. C., Guglielmetti, R., Eds.; Plenum Press: New York, 1999; Vol. 2, pp 9−63. (d) Ichimura, K. *Chem. Rev.* **2000**, *100*, 1847−1873.

10.1021/jo051417w CCC: $30.25
Published on Web 08/25/2005

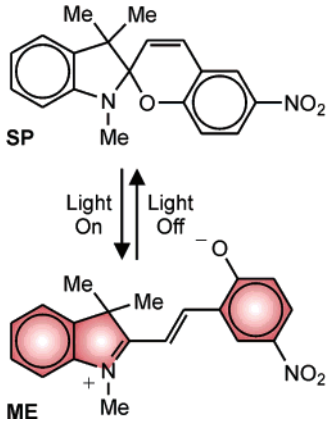

FIGURE 1. Interconversion of a colorless spiropyran (**SP**) and a colored merocyanine (**ME**).

formations translate also into significant dipole moment and molecular polarizability alterations. In fact, diverse photoresponsive materials have been designed around the unique properties of this class of photochromic compounds over the past three decades.[1b,6−12] Their preparation generally relies on the integration of nitrospiropyrans within polymer matrixes, multilayer structures, or liquid-crystalline assemblies. The macroscopic properties of the resulting composites can then be regulated by operating their photochromic components with optical stimulations. Indeed, the birefringence, color, dichroism, and/or refractive index of materials based on nitrospiropyrans have all been modulated successfully, relying on these operating principles.

The photoinduced isomerization of nitrospiropyrans to the corresponding merocyanines demands the cleavage of the C−O bond at the spirocenter and the subsequent cis → trans isomerization of the adjacent C=C bond. In organic solvents at ambient temperature, the first of these two steps occurs upon ultraviolet excitation with picosecond time scales[13−16] along the potential energy surface of the first triplet state.[17,18] Indeed, the nitro group appended to the benzopyran fragment facilitates intersystem crossing in the spiropyran geometry. Concomitantly, the small dihedral angle (15−30°) between the axis of the $2p_z$ orbital on the indoline nitrogen atom and that of the adjacent σ_{C-O} orbital encourages electronic mixing and C−O bond cleavage.[2] The resulting ring-opened intermediate decays to the ground state with microsecond time scales, producing a mixture of *cis*- and *trans*-merocyanines.[17] The subsequent ground-state cis → trans isomerization completes the photoinduced process in submillisecond time scales.[17]

The participation of a triplet state with microsecond lifetime in the isomerization of nitrospiropyrans[18] opens competitive reaction pathways.[19] These side reactions are often irreversible and are responsible for the characteristic photodegradation of nitrospiropyrans.[3,5] In particular, the relatively long-lived triplet state encourages the production of significant amounts of singlet oxygen ($^1\Delta_g$),[17f,g] which, presumably, causes the oxidative degradation of the photochromic species. Consistently, the fatigue resistances of nitrospiropyrans increase considerably in the presence of singlet-oxygen scavengers.[20,21]

The photogenerated and colored merocyanines are not thermally stable.[1−5] They revert to the original and colorless forms after a rate-determining[22] trans → cis reisomerization and the subsequent re-formation of the C−O bond at the spirocenter. Thus, the macroscopic properties (e.g., color and/or refractive index) of a nitrospiropyran-based material can be switched reversibly between two states by simply turning on and off an optical stimulation. The thermal decoloration process, however, is relatively slow. In organic solvents at ambient temperature, the lifetimes of the colored isomers range from 1 to 10^4 s.[17c,e,g] It follows that the switching speeds of photoresponsive materials based on these compounds cannot be greater than 1 Hz.

The poor fatigue resistances and slow switching speeds of photoresponsive materials based on nitrospiropyrans have limited considerably their practical applications.[1b,6−12] The detailed knowledge established on the fundamental properties of these compounds,[13−22] however, can be exploited to engineer photochromic compounds with improved isomerization kinetics and stability. In search of viable strategies to optimize both parameters, we have designed a new family of heterocyclic photochromes closely related to nitrospiropyrans.[23] In this article, we report the synthesis, structural characterization, and

(7) Crano, J. C.; Kwak, W. S.; Welch, C. N. In *Applied Photochromic Polymer Systems*; McArdle, C. B., Ed.; Blackie: Glasgow, 1992; pp 31−79.
(8) (a) Krongauz, V. In *Applied Photochromic Polymer Systems*; McArdle, C. B., Ed.; Blackie: Glasgow, 1992; pp 121−173. (b) Berkovic, G.; Krongauz, V.; Weiss, V. *Chem. Rev.* **2000**, *100*, 1741−1754.
(9) Irie, M. In *Applied Photochromic Polymer Systems*; McArdle, C. B., Ed.; Blackie: Glasgow, 1992; pp 174−206.
(10) Hibino, J.; Hashida, T.; Suzuki, M. In *Photo-Refractive Materials for Ultrathin Density Optical Memory*; Irie, M., Ed.; Elsevier: Amsterdam, 1994; pp 25−53.
(11) Kawata, S.; Kawata, Y. *Chem. Rev.* **2000**, *100*, 1777−1788.
(12) Delaire, J. A.; Nakatani, K. *Chem. Rev.* **2000**, *100*, 1817−1845.
(13) (a) Krysanov, S. A.; Alfimov, M. V. *Chem. Phys. Lett.* **1982**, *91*, 77−80. (b) Krysanov, S. A.; Alfimov, M. V. *Laser Chem.* **1984**, *4*, 129−138.
(14) Kalisky, Y.; Orlowski, T. E.; Williams, D. J. *J. Phys. Chem.* **1983**, *87*, 5333−5338.
(15) (a) Ito, T.; Hiramatsu, M.; Hirano, I.; Ohtani, H. *Macromolecules* **1990**, *23*, 4528−4532. (b) Ito, T.; Hiramatsu, M.; Hosoda, M.; Tsuchiya, Y. *Rev. Sci. Instrum.* **1991**, *62*, 1415−1419.
(16) Ernsting, N. P.; Arthen-Engeland, T. *J. Phys. Chem.* **1991**, *95*, 5502−5509.
(17) (a) Atabekyan, L. S.; Chibisov, A. K. *Zh. Prikl. Spektrosk.* **1987**, *46*, 651−654. (b) Görner, H.; Atabekyan, L. S.; Chibisov, A. K. *Chem. Phys. Lett.* **1996**, *260*, 59−64. (c) Görner, H. *Chem. Phys.* **1997**, *222*, 315−329. (d) Chibisov, A. K.; Görner, H. *J. Photochem. Photobiol., A* **1997**, *105*, 261−267. (e) Chibisov, A. K.; Görner, H. *J. Phys. Chem. A* **1997**, *101*, 4305−4312. (f) Görner, H. *Chem. Phys. Lett.* **1998**, *282*, 381−390. (g) Görner, H. *Phys. Chem. Chem. Phys.* **2001**, *3*, 416−423.
(18) Quenching and sensitization experiments, coupled with the investigation of the photoinduced re-isomerization of the colored isomers, demonstrate the fundamental role of the triplet state in the photoisomerization of nitrospiropyrans (ref 17). Earlier reports, however, suggest alternative mechanisms for these photoinduced transformations. See refs 13−15 and (a) Irie, M.; Menju, A.; Hayashi, K. *Macromolecules* **1979**, *12*, 1176−1180. (b) Krongauz, V.; Kiwi, J.; Grätzel, M. *J. Photochem.* **1980**, *13*, 89−97. (c) Kalisky, Y.; Williams, D. J. *Macromolecules* **1984**, *17*, 292−296. (d) Lenoble, C.; Becker, R. S. *J. Phys. Chem.* **1986**, *90*, 62−65. (e) Tamaki, T.; Sakuragi, M.; Ichimura, K.; Aoki, K. *Chem. Phys. Lett.* **1989**, *161*, 23−26.
(19) Malkin, Y. N.; Krasieva, T. B.; Kuzmin, V. A. *J. Photochem. Photobiol., A* **1989**, *49*, 75−88.
(20) Sakuragi, M.; Aoki, K.; Tamaki, T.; Ichimura, K. *Bull. Chem. Soc. Jpn.* **1990**, *63*, 74−79.
(21) Salemi, C.; Giusti, G.; Guglielmetti, R. *J. Photochem. Photobiol., A* **1995**, *86*, 247−252.
(22) Sheng, Y.; Leszczynski, J.; Garcia, A. A.; Rosario, R.; Gust, D.; Springer, J. *J. Phys. Chem. B* **2004**, *108*, 16233−16243.
(23) Tomasulo, M.; Sortino, S.; Raymo, F. M. *Org. Lett.* **2005**, *7*, 1109−1112.

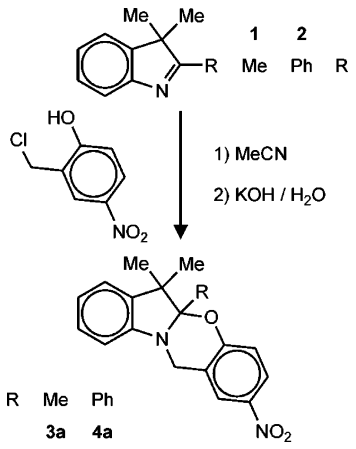

FIGURE 2. Synthesis of the [1,3]oxazines **3a** and **4a**.

photochemical properties of two members of this novel class of photoactive molecular switches.

Results and Discussion

Design and Synthesis. The photoinduced transformation of **SP** into **ME** (Figure 1) requires submillisecond time scales to reach completion at ambient temperature in organic solvents.[17] The ground-state cis → trans isomerization of the C=C bond linking the indoline and 4-nitrophenolate fragments of the ring-opened form limits the rate of the overall process.[17,22] The thermal transformation of **ME** into **SP** requires several minutes under the same experimental conditions.[17] Once again, the trans → cis isomerization of the C=C bond limits the rate of this transformation.[22] Thus, the coloration and decoloration kinetics can both be improved by removing the C=C bond from the nitrospiropyran skeleton. Indeed, the sluggish cis/trans interconversion steps are not strictly necessary to generate a significant absorbance change in the visible region. The photoinduced and fast cleavage of the C−O bond at the spirocenter alone is sufficient to produce a 4-nitrophenolate chromophore able to absorb visible light. Under these conditions, the thermal and fast re-formation of the C−O bond is the only requirement to restore the original and colorless form.

On the basis of these considerations, we have designed and synthesized the two compounds **3a** and **4a** (Figure 2). Specifically, the N-alkylation of the indoles **1** and **2** with 2-chloromethyl-4-nitrophenol and the subsequent cyclization under basic conditions led to the target molecules **3a** and **4a** in an overall yield of 58%. These two compounds differ in the group on the tetrahedral carbon atom shared by the indoline and benzooxazine fragments. The relative orientation of these two fused heterocycles constrains the dihedral angle between the axis of the $2p_z$ orbital on the indoline nitrogen atom and that of the adjacent σ_{C-O} orbital to values comparable to those (15−30°) of nitrospiropyrans.[2] Thus, this particular geometry is expected to favor electronic mixing between the two orbitals and facilitate the cleavage of the C−O bond in the excited state, as observed for nitrospiropyrans.[2] It follows that the ultraviolet excitation of either **3a** or **4a** should open the central [1,3]oxazine ring to generate a 4-nitrophenolate chromophore able to absorb visible light.

^{1}H NMR Spectroscopy. The chiral center at the junction of the two heterocycles in **3a** and **4a** imposes two distinct environments on the pair of indoline methyl groups and on the two oxazine methylene protons. Consistently, the ^{1}H NMR spectra of both compounds reveal pairs of singlets for the methyl protons and AB systems for the methylene protons, when recorded in acetonitrile-d_3 at ambient temperature. For example, the two singlets for the methyl protons (Me$^{\circ}$ and Me$^{\square}$) of **3a** appear at 1.15 and 1.51 ppm in the ^{1}H NMR spectrum (a in Figure 3) recorded at 275 K. The AB system for the methylene protons (H$^{\circ}$ and H$^{\square}$) is instead centered at 4.69 ppm. Upon warming the solution, we found that the two singlets broaden (b−f in Figure 3) and eventually coalesce into a single peak. Similarly, the two doublets within the AB system broaden and coalesce into a single peak. These changes are a result of the interconversion between the two enantiomers of **3a** on the ^{1}H NMR time scale. This degenerate site exchange process demands the thermal cleavage of the C−O bond at the junction of the two heterocycles with the formation of the ring-opened intermediate **3b** (Figure 3). The kinetic parameters (Table 1) associated with the ring-opening process can be extracted from the analysis of the temperature dependence of the line widths associated with the singlets for Me$^{\circ}$ and Me$^{\square}$ in the slow-exchange regime.[24] A similar analysis can be extended to the ^{1}H NMR spectra (Figure S2) of **4a**, which reveal essentially the same behavior.

A comparison of the rate constants (k in Table 1) determined for the thermal ring opening of **3a** and **4a** in acetonitrile-d_3 reveals that the group on the chiral center at the junction of the two heterocycles has a pronounced influence on the kinetics of this process. Indeed, a transition from the methyl group of **3a** to the phenyl ring of **4a** translates into a decrease in k from ca. 199 to 0.4 s^{-1}. This change corresponds to an increase in free energy barrier ($\Delta G^{\ddagger}$ in Table 1) of ca. 3.7 kcal mol^{-1}. Interestingly, the enthalpic term ($\Delta H^{\ddagger}$ in Table 1) dominates $\Delta G^{\ddagger}$, while the entropic contribution ($T\Delta S^{\ddagger}$) at 298 K is less than 1 kcal mol^{-1} for both compounds. In toluene-d_8, $T\Delta S^{\ddagger}$ remains negligible, but $\Delta H^{\ddagger}$ increases by ca. 4.7 kcal mol^{-1} for **3a**. Consistent with the solvent-induced enhancement in $\Delta H^{\ddagger}$, the ^{1}H NMR spectrum of **4a** does not change significantly with temperature in toluene-d_8. Two well-defined singlets for the methyl protons of **4a** can clearly be observed even at 363 K, in agreement with the slow ring-opening kinetics.

The ring-opened intermediates **3b** (Figure 3) and **4b** (Figure S2) revert to the corresponding oxazines **3a** and **4a** after the intramolecular attack of the 4-nitrophenolate

(24) Below the coalescence temperature, two well-separated singlets can be observed for the methyl protons Me$^{\circ}$ and Me$^{\square}$ in the ^{1}H NMR spectra (a−c in Figure 3). Under these conditions, the line width ($\Delta\nu$) of either one of the two singlets is related to the rate constant (k) of the degenerate site exchange process according to eq 1, where $\Delta\nu_0$ is the line width at the stopped-exchange limit (Nelson, J. H. *Nuclear Magnetic Resonance Spectroscopy*; Prentice Hall: Upper Saddle River, NJ, 2003.). Following this protocol, k can be determined at any temperature (T) within the slow-exchange regime. A plot of $\ln(kT^{-1})$ against T^{-1} can then be fitted to eq 2, where R is the gas constant, to extract the enthalpy ($\Delta H^{\ddagger}$) and entropy ($\Delta S^{\ddagger}$) of activation. Finally, the free energy ($\Delta G^{\ddagger}$) of activation can be calculated at any T using eq 3.

$$k = \pi(\Delta\nu - \Delta\nu_0) \quad (1)$$

$$\ln\frac{k}{T} = -\frac{\Delta H^{\ddagger}}{RT} + \frac{\Delta S^{\ddagger}}{R} + 23.76 \quad (2)$$

$$\Delta G^{\ddagger} = \Delta H^{\ddagger} - T\Delta S^{\ddagger} \quad (3)$$

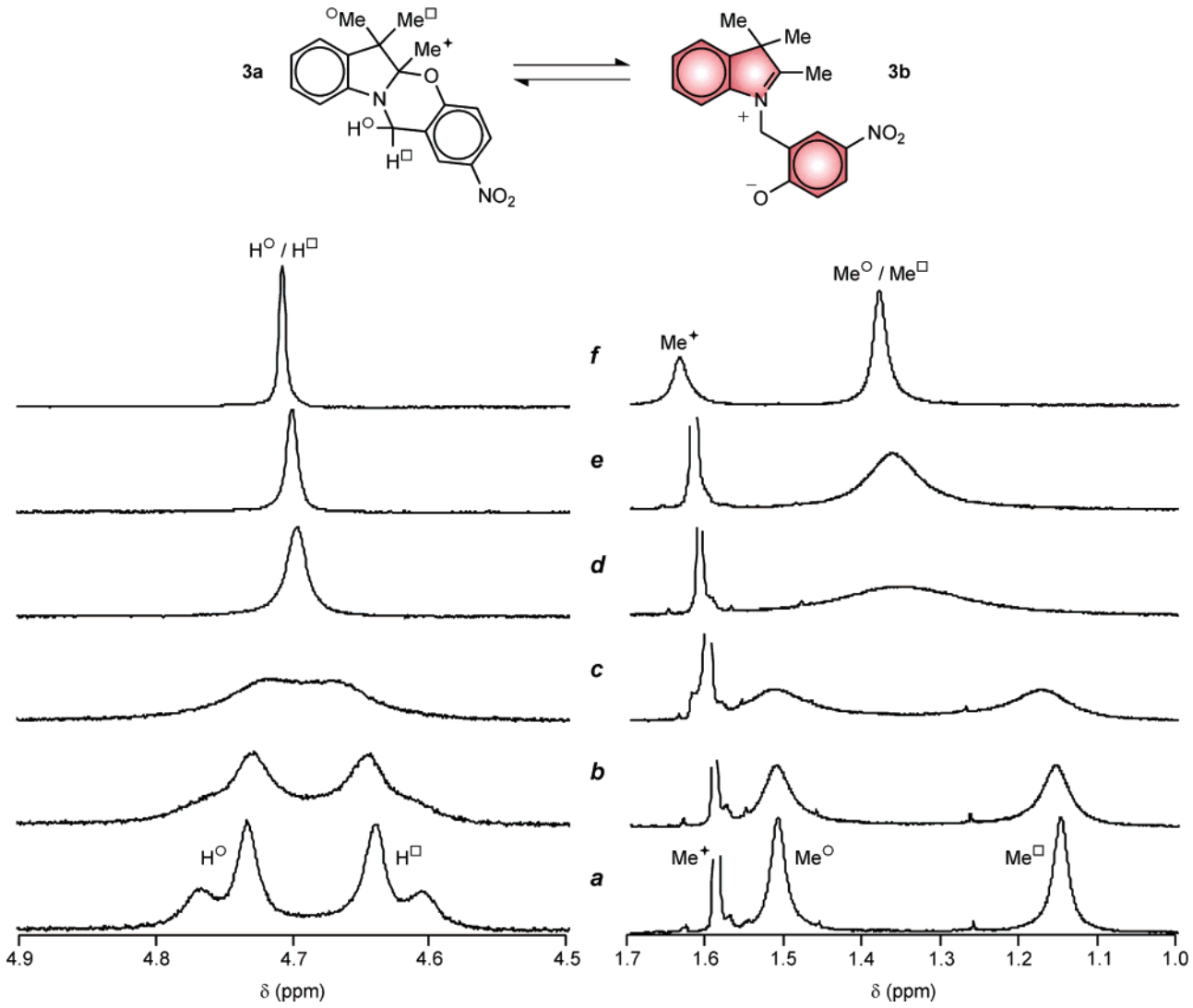

FIGURE 3. Partial ^{1}H NMR spectra (500 MHz, acetonitrile-d_3, 5 mM) of **3a** at 275 (a), 283 (b), 293 (c), 313 (d), 323 (e), and 336 K (f).

TABLE 1. Kinetic Parameters Associated with the Thermal Ring Opening of 3a and 4a at 298 K[a]

solvent	compound	k (s^{-1})	$\Delta G^{\ddagger}$ (kcal mol^{-1})	$\Delta H^{\ddagger}$ (kcal mol^{-1})	$-\Delta S^{\ddagger}$ (kcal mol^{-1} K^{-1})
acetonitrile-d_3	**3a**	199 ± 7	14.31 ± 0.02	13.5 ± 0.2	0.003 ± 0.001
	4a	0.4 ± 0.1	17.99 ± 0.18	17.4 ± 0.3	0.002 ± 0.001
toluene-d_8[b]	**3a**	0.081 ± 0.036	19.00 ± 0.29	19.8 ± 2.0	−0.003 ± 0.006

[a] The rate constant (k), free energy ($\Delta G^{\ddagger}$), enthalpy ($\Delta H^{\ddagger}$), and entropy ($\Delta S^{\ddagger}$) of activation were determined by variable-temperature ^{1}H NMR spectroscopy (ref 24). [b] In toluene-d_8, the line widths of the singlets associated with the pair of methyl protons of **4a** remain approximately constant in the examined temperature range (275−363 K). As a result, the kinetic parameters for the ring opening of this compound could not be determined.

anion to the adjacent indolium cation. Nucleophiles able to compete intermolecularly with the ring-closing step can therefore "trap" these short-lived intermediates. For example, the addition of 2 equiv of Bu_4NOH to a solution of **4a** results in the quantitative formation of the hemiaminal **4c** (Figure 4). This transformation is accompanied by pronounced changes in the ^{1}H NMR spectrum (a and b in Figure 4). In particular, the doublet for H^a moves from 7.99 to 8.14 ppm, while the resonances for all the other aromatic protons move in the opposite direction. The largest chemical shift change is observed for the doublet associated with H^h, which moves from 6.96 to 6.11 ppm. The AB system for the pair of diastereotopic methylene protons H^l and H^m is retained with the transformation of **4a** into **4c**, consistent with the presence of a chiral center in both compounds. In addition, the formation of **4c** is further confirmed by the presence of a peak at an *m/z* of 390 in the fast atom bombardment mass spectrum.

The addition of Bu_4NOH to a solution of **3a** has similar effects on the ^{1}H NMR and mass spectra. Once again, peaks for the corresponding hemiaminal **3c** (Figure S3) can be clearly observed. The methyl group in position 2 of the indolium fragment of **3b**, however, is relatively acidic. Thus, the nucleophilic attack of the hydroxide anion to the indolium cation of **3b** competes with its

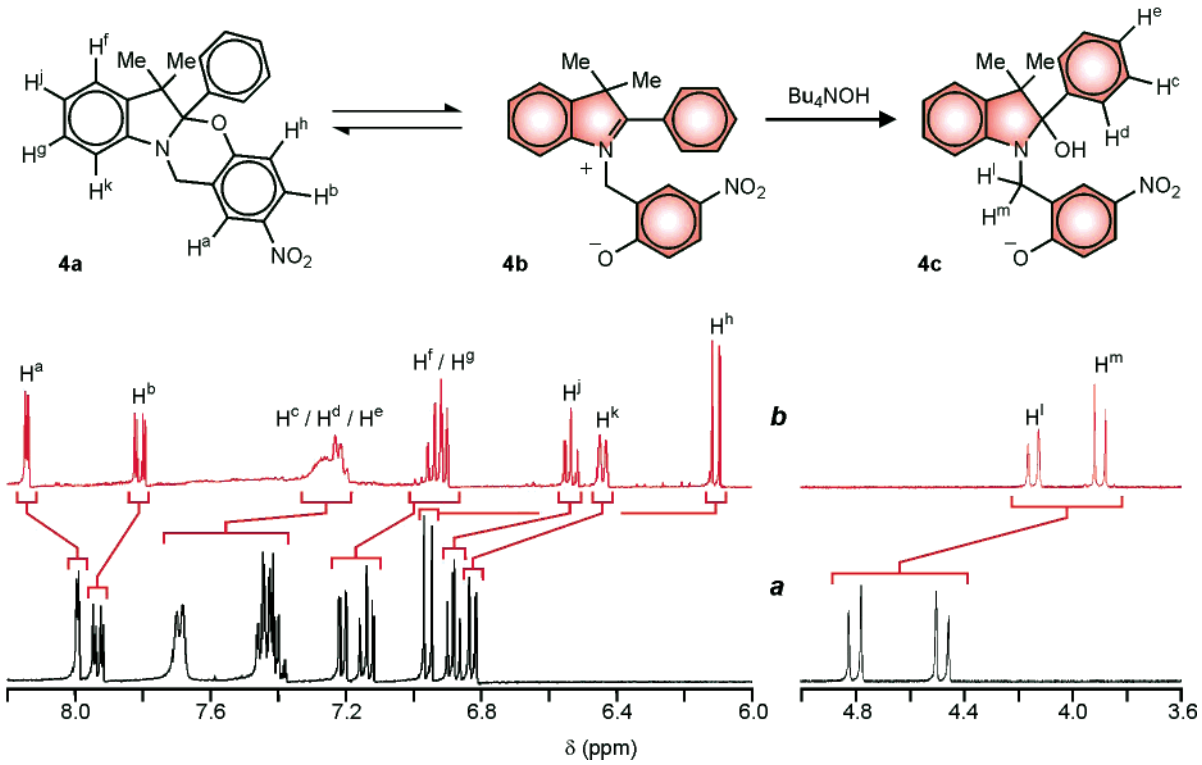

FIGURE 4. Partial ^{1}H NMR spectra (400 MHz, acetonitrile-d_3, 10 mM) of **4a** before (a) and after (b) the addition of Bu_4NOH (2 equiv).

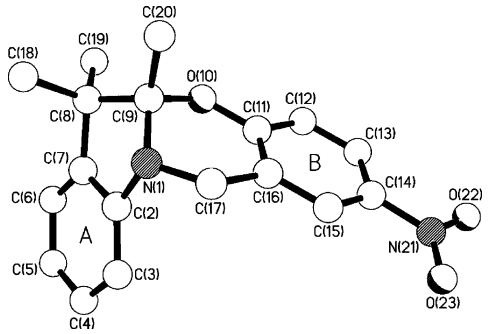

FIGURE 5. Single-crystal X-ray structure of **3a**.

deprotonation, and the compound **3d** (Figure S3) is formed in parallel to the hemiaminal **3c**. Consistently, the broad resonance for the pair of diastereotopic methylene protons of **3a** (a in Figure S3) is replaced by an AB system for H^a and H^b of **3c** and a singlet for H^A and H^B of **3d** (b in Figure S3). In addition, an AB system for the olefinic protons H^C and H^D of **3d** can also be observed. From the integrals of these resonances, the ratio between **3c** and **3d** can be estimated to be 34:66.

X-ray Crystallography. The single-crystal X-ray structure of **3a** (Figure 5) shows a near-orthogonal arrangement for the fused indoline and benzooxazine ring systems, their planes, excluding the two junction atoms [C(9) and N(1)], being inclined by ca. 87°. Both ring systems adopt envelope-type geometries, with that for the indoline moiety the chiral carbon C(9) being ca. 0.50 Å out of the plane of the remaining indoline atoms (which are coplanar to better than 0.01 Å), while for the benzooxazine unit the nitrogen center N(1) lies ca. 0.53 Å out of the plane of the remaining benzooxazine atoms (which are coplanar to within ca. 0.08 Å). The geometry at N(1) is pyramidal, the nitrogen lying ca. 0.36 Å out of the plane of its substituents, and its $2p_z$ orbital is approximately collinear with the σ-orbital of the C(9)−O(10) bond, the O(10)−C(9)−N(1) lone-pair dihedral angle being ca. 9°.

Adjacent molecules in the crystal are linked by a combination of C−H···π, π···π, and C−H···O interactions. One face of the indoline C_6 ring (ring **A** in Figure 5) is approached by a hydrogen atom of the benzooxazine C_6 ring (ring **B**) [H···**A** 2.97 Å, C(13)−H···**A** 128°]. The other face is close to a proton on C(20) [H···**A** 2.99 Å, C(20)−H···**A** 132°]. These two C−H···π interactions subtend an angle of ca. 176° at the centroid of ring **A**. One face of ring **B** is approached by a proton on C(18) [H···**B** 3.13 Å, C(18)−H···**B** 173°], while the other face is involved in a head-to-tail overlap with the nitro group of its centrosymmetrically related counterpart. The corresponding N···centroid and mean interplanar separations are 3.67 and 3.57 Å, respectively. The oxygen atoms of the nitro group are the recipients of a pair of weak C−H···O interactions. The aromatic C(3) proton approaches O(23) [H···O 2.48 Å, C−H···O 176°], while a proton on C(20) is close to O(22) [H···O 2.65 Å, C−H···O 174°].

The single-crystal X-ray structure of **4c** (Figure 6) confirms the opening of the oxazine ring. As was seen in **3a**, the indoline fragment of **4c** adopts an envelope-type geometry, the chiral center C(9) being ca. 0.52 Å out of the plane of the remaining indoline atoms (which are coplanar to within ca. 0.02 Å). The geometry at the adjacent nitrogen atom [N(1)] is again pyramidal, the nitrogen lying ca. 0.33 Å out of the plane of its substituents. Despite the oxazine ring having been opened, the nitrogen $2p_z$ orbital and the σ-orbital of the C(9)−O(20)

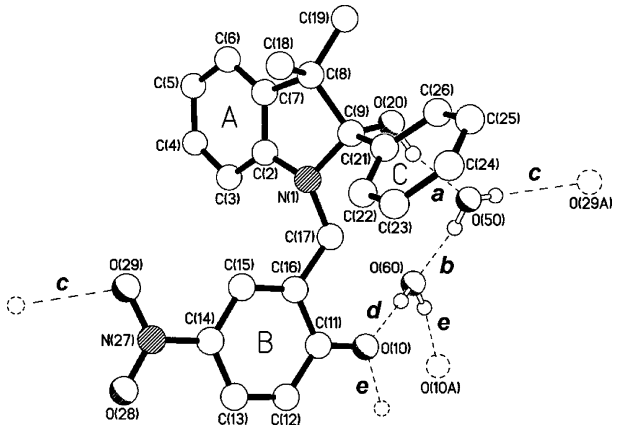

FIGURE 6. Single-crystal X-ray structure of **4c** showing O−H···O hydrogen-bonding interactions with included water molecules. The O−H···O hydrogen-bonding geometries [O···O, H···O (Å), and O−H···O (°)] are: (a) 2.859(2), 2.00, 160.0; (b) 2.687(3), 1.81, 164; (c) 3.135(3), 2.35, 146; (d) 2.773(3), 1.88, 170; (e) 2.760(3), 1.87, 168.

bond are still approximately collinear, the O(20)−C(9)−N(1) lone-pair dihedral angle being ca. 11°.

The packing of **4c** in the crystal is dominated by O−H···O hydrogen bonds involving the included water molecules (Figure 6). There are, however, some relatively weak C−H···π interactions between the anion in **4c** and the included Bu_4N^+ cation, with both faces of ring **A** [H···**A** 3.31 Å, C−H···**A** 143°; H···**A** 3.47 Å, C−H···**A** 130°; H···**A**···H 158°] and ring **B** [H···**B** 2.97 Å, C−H···**B** 160°; H···**B** 3.39 Å, C−H···**B** 130°; H···**B**···H 118°] being approached by methylene protons. Ring **C** is only approached on one face [H···**C** 2.97 Å, C−H···**C** 152°], presumably because the other face is partially shielded by the adjacent methyl group [C(18)].

Molecular Modeling. To gain further understanding on the thermal isomerization of our oxazines, we have modeled the ground-state potential energy surface of **3a** with a combination of AM1 (Figure S6) and B3LYP/6-31G(d) calculations. In the B3LYP/6-31G(d) geometry of **3a** (Figure 7), the length of the C−O bond at the junction of the two heterocycles is 1.470 Å. The cleavage of this bond proceeds through a transition state that is 18.1 kcal mol^{-1} higher in energy than **3a**. This activation energy is close to the experimental $\Delta H^{\ddagger}$ (Table 1) determined for the very same process in toluene-d_8. According to our calculations, the ring-opened product **3b** is 17.6 kcal mol^{-1} higher in energy than **3a**. Thus, the ring-closing reaction has an energy barrier of only 0.5 kcal mol^{-1}.

Steady-State Absorption Spectroscopy. The two chromophoric fragments of **3a** and **4a** are isolated electronically. As a result, their absorption spectra (a in Figures 8 and S7) resemble the sum of those (b and c in Figures 8 and S7) of model indolines (**5** and **6** in Table 2) and 4-nitroanisole (**7** in Table 2). The most significant difference is a shift to longer wavelengths for the absorption associated with the 4-nitrophenyl chromophore. This band is centered at 307 nm in the spectrum of **7** (Table 2), but at 318 and 316 nm in those of **3a** and **4a**, respectively.

The spectra of **3a** and **4a** (a in Figures 8 and S7) do not show bands in the wavelength range expected for a 4-nitrophenolate chromophore (e in Figures 8 and S7).

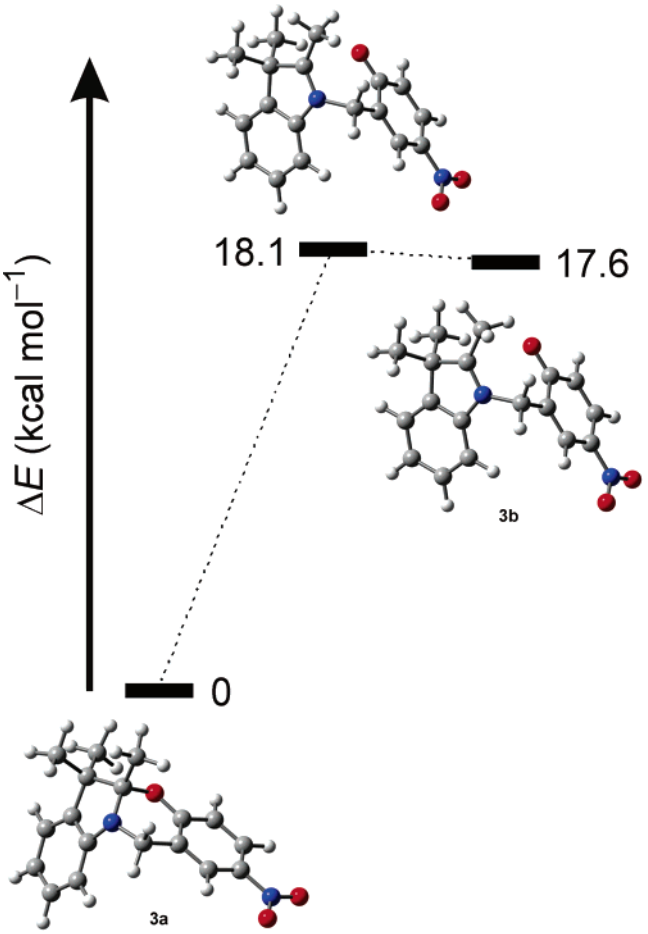

FIGURE 7. Zero-point corrected energies [B3LYP/6-31G(d)] of the main stationary points on the ground-state potential energy surface of **3a**.

Thus, the stationary concentrations of the ring-opened isomers **3b** and **4b** are below the detection limit in both cases, under these experimental conditions (MeCN, 298 K). After the addition of Bu_4NOH to solutions of **3a** and **4a**, however, a band at ca. 430 nm appears in the spectra of both species (d in Figures 8 and S7). This band resembles the absorption (e in Figures 8 and S7) of the model phenolate **8** (Table 2) and can be assigned to the ring-opened products **3c/3d** and **4c** detected by ^{1}H NMR spectroscopy (Figures 4 and S3).

Transient Absorption Spectroscopy. The transient absorption spectra, recorded 30 ns after laser excitation, of aerated MeCN solutions of **3a** and **4a** show bands centered at ca. 440 nm (a in Figures 9 and S8). In both instances, the transient bands resemble the steady-state ones (b in Figures 9 and S8) of **3c/3d** and **4c** and, therefore, can be assigned to ground-state absorptions of the 4-nitrophenolate chromophores of **3b** and **4b**. In agreement with this assignment, singlet-oxygen measurements for **4a** and control experiments with **7** confirm that the transient absorptions are not associated with a triplet−triplet transition. Indeed, the quantum yield of singlet oxygen is less than 0.02, and the transient spectrum of **7** does not reveal any detectable absorption in the nanosecond domain.[25]

The kinetic traces monitored at 440 nm (c in Figures 9 and S8) indicate that the ring-opened isomers are

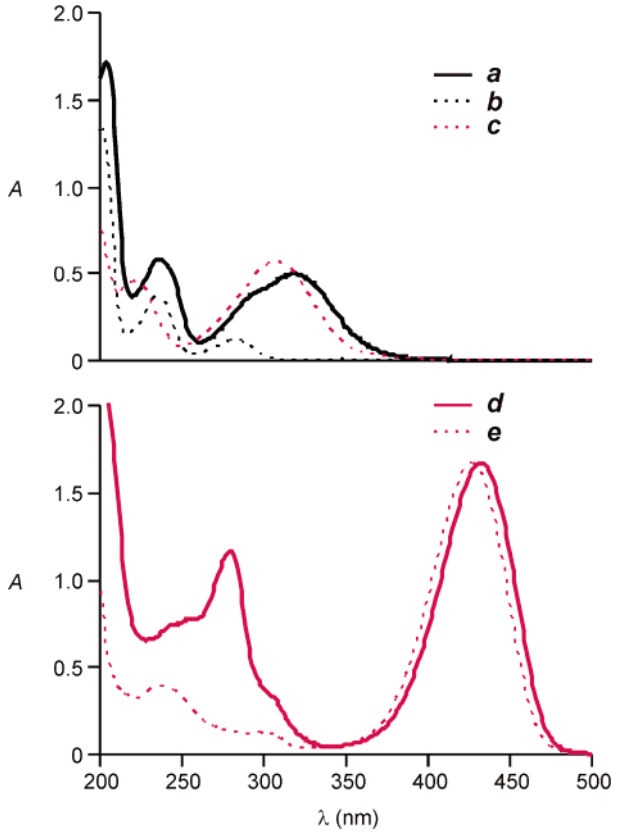

FIGURE 8. Steady-state absorption spectra (0.1 mM, MeCN, 298 K) of **3a** (a), **5** (b), and **7** (c) as well as of **3a** after the addition of Bu_4NOH (1 equiv) (d) and **8** (e).

TABLE 2. Absorption Wavelengths (λ) and Molar Extinction Coefficients (ϵ) of the Oxazines 3a and 4a and of the Model Compounds 5−8 in MeCN at 298 K[a]

compound	λ (nm)	ϵ (mM^{-1} cm^{-1})
3a	318	10.0 ± 0.5
4a	316	11.0 ± 0.6
5	283	2.2 ± 0.1
6	281	3.9 ± 0.2
7	307	11.1 ± 0.6
8	426	32.5 ± 0.9

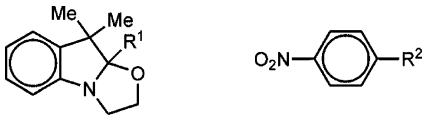

R1 Me Ph
5 6

R2 OMe O⁻
7 8

[a] The model compounds are shown in the following diagram. The λ and ϵ of the phenolate **8** were determined by recording the absorption spectrum of the corresponding phenol in the presence of Bu_4NOH (4 equiv).

formed within the excitation pulse (ca. 6 ns). The corresponding quantum yields can be estimated to be 0.03 for **3b** and 0.1 for **4b**. In both instances, the absorbance decays monoexponentially to zero (d in Figures 9 and S8) with a first-order rate constant of ca. 4×10^7 s^{-1}, as the ring-opened isomers **3b** and **4b** revert thermally to the

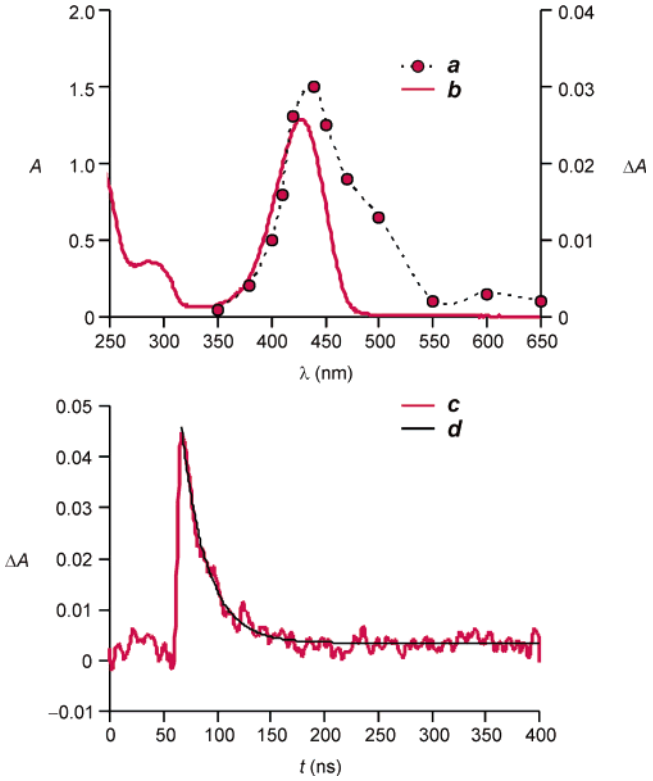

FIGURE 9. Transient absorption spectrum (a) of **4a** recorded 30 ns after the laser pulse (355 nm, 6 ns, 8 mJ, 0.1 mM, MeCN, 295 K) and steady-state absorption spectrum (b) of **4a** and 100 equiv of Bu_4NOH (0.1 mM, MeCN, 298 K). Evolution of the absorbance at 440 nm (c) upon laser excitation of **4a** and the corresponding monoexponential curve fitting (d).

original oxazines **3a** and **4a**. Thus, the photoinduced and reversible interconversion between the two isomers of each system can be achieved with nanosecond switching speeds. Furthermore, both photochromic switches are remarkably stable. In fact, the steady-state absorption spectra of **4a** recorded before and after 3000 excitation cycles, operated in the presence of molecular oxygen, are virtually identical.

The steady-state absorption spectra (a in Figures 10 and S9) of poly(methyl methacrylate) (PMMA) films doped with **3a** or **4a** are essentially identical to those recorded in MeCN (a in Figures 8 and S7). Once again, the stationary concentrations of the ring-opened isomers **3b** and **4b** are negligible, and the absorption bands of their 4-nitrophenolate chromophores cannot be detected. In the presence of Bu_4NOH, however, the characteristic absorptions of **3c/3d** and **4c** at ca. 430 nm can be observed also in PMMA (b in Figures 10 and S9). Similar bands are evident in the transient absorption spectra of **3a** and **4a** (c in Figures 10 and S9) recorded 1 μs after laser excitation. These absorptions can be assigned to the photogenerated ring-opened isomers **3b** and **4b** and are relatively short-lived.[26] After 80 μs, for example, the band at 430 nm can no longer be observed in the transient spectrum of **4a** (d in Figure 10). In addition to this absorption, a second and more intense band at 380 nm

(25) The lowest triplet state of 4-nitroanisole has a subnanosecond lifetime in MeCN. Mir, M.; Jansen, L. M. G.; Wilkinson, F.; Bourdelande, J. L.; Marquet, J. *J. Photochem. Photobiol., A* **1998**, *113*, 113−117.

(26) The transient absorptions of **3a** and **4a** at 430 nm appear to decay biexponentially (Figure S10). However, the signal-to-noise ratio of the kinetic traces is relatively poor, and a reliable determination of the associated rate constants was not possible.

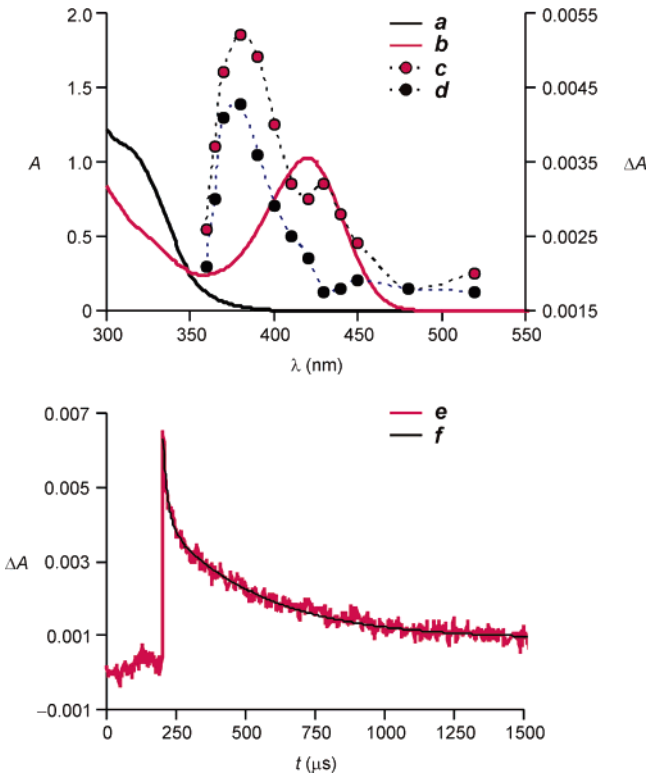

FIGURE 10. Steady-state absorption spectra (5%, PMMA, 298 K) of **4a** without (a) and with (b) Bu_4NOH (7 equiv) and transient absorption spectra of **4a** recorded 1 (c) or 80 μs (d) after the laser pulse (355 nm, 6 ns, 12 mJ, 5%, PMMA, 295 K). Evolution of the absorbance at 380 nm (e) upon laser excitation of **4a** (355 nm, 6 ns, 12 mJ, 5%, PMMA, 295 K) and the corresponding biexponential curve fitting (f).

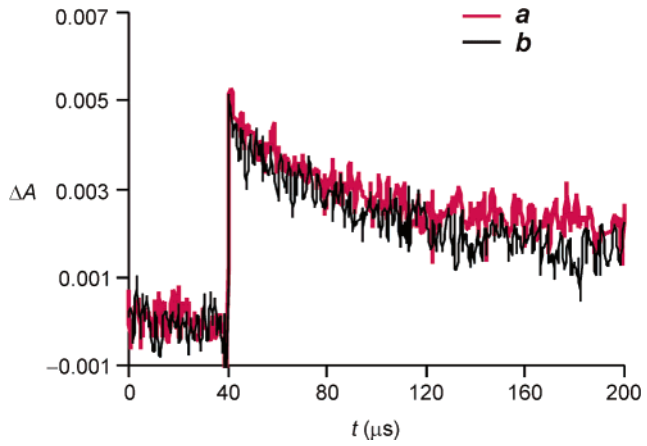

FIGURE 11. Evolution of the absorbance at 380 nm upon laser excitation of **4a** (355 nm, 6 ns, 12 mJ, 5%, PMMA, 295 K) before (a) and after (b) 1000 excitation cycles.

(c in Figures 10 and S9) is evident in the transient spectra of both compounds. This absorption is relatively long-lived and can still be observed after the complete decay of the band at 430 nm (d in Figure 10). The corresponding kinetic traces (e in Figure 10 and d in Figure S9) show biexponential decays with rate constants of 1×10^4 and 1×10^5 s^{-1} for **3a** and of 3×10^3 and 5×10^4 s^{-1} for **4a**. Both trends parallel the behavior of nitrospiropyrans in polymer matrixes.[8,27] Indeed, the thermal decoloration of nitrospiropyrans also follows biexponential kinetics under these experimental conditions. The aggregation of their photogenerated isomers into long-lived supramolecular assemblies is believed to be responsible for this behavior. Presumably, similar processes govern the spectral evolution of **3a** and **4a** in PMMA. In any case, the absorbance associated with the photogenerated species of both systems can be modulated reversibly with millisecond switching speeds. Once again, both photochromic switches are remarkably stable and remain essentially unaffected after thousands of excitation cycles. As an example, Figure 11 illustrates kinetic traces recorded at 380 nm for **4a** before and after 1000 switching cycles. The two profiles are virtually indistinguishable, indicating that the photochromic switch is, indeed, extremely stable.

Conclusions

Indoline and benzooxazine fragments can be conveniently fused in a single synthetic step starting from 2-*R*-3,3′-dimethyl-3*H*-indoles and 2-chloromethyl-4-nitrophenol. The [1,3]oxazine ring in the resulting molecules opens thermally with a free energy barrier ranging from 14 to 19 kcal mol^{-1}. This parameter is dominated by its enthalpic term and increases when *R* is changed from a methyl to a phenyl group and when the solvent varies from acetonitrile-d_3 to toluene-d_8. The fast re-isomerization of the ring-opened species translates into a negligible steady-state concentration. However, this isomer can be trapped chemically and characterized in this form by nuclear magnetic resonance spectroscopy, crystallography, and visible absorption spectroscopy. Indeed, the nucleophilic attack of a hydroxide anion to the indolium cation of the ring-opened species prevents the thermal re-isomerization.

The ultraviolet absorption spectra of these compounds indicate that the indoline and benzooxazine chromophores are electronically isolated. The local excitation of the benzooxazine fragment at 355 nm cleaves its C−O bond at the junction of the two heterocycles in less than 6 ns with a quantum yield up to 0.1. The photoinduced bond cleavage generates a 4-nitrophenolate chromophore with an intense absorption at 440 nm. The photogenerated isomer reverts thermally to the original [1,3]oxazine with a lifetime of 22 ns. These processes can be reproduced successfully even in poly(methyl methacrylate) matrixes. Under these conditions, however, the thermal re-isomerization occurs in submillisecond time scales with biexponential kinetics. Presumably, the aggregation of the photogenerated isomer within the polymer matrix is responsible for this behavior. Even in the presence of molecular oxygen, the photoinduced isomerization and thermal re-isomerization are not accompanied by any detectable degradation. These molecules withstand thousands of excitation cycles without any sign of decomposition in aerated acetonitrile as well as in poly(methyl methacrylate) matrixes.

The fast isomerization kinetics and excellent fatigue resistance of our oxazines offer the opportunity to modulate rapidly and efficiently molecular (e.g., dipole moment) and macroscopic (e.g., color) properties under the

(27) Krongauz, V. A. In *Photochromism: Molecules and Systems*; Dürr, H., Bouas-Laurent, H., Eds.; Elsevier: Amsterdam, 1990; pp 793−821.

influence of optical stimulations. In fact, our molecular design can lead to the development of a new family of photochromic compounds with unprecedented switching speeds and remarkable stability and, eventually, evolve into photonic materials with unique photoresponsive character.

Experimental Section

2-Nitro-5a,6,6-trimethyl-5a,6-dihydro-12*H*-indolo[2,1-b][1,3]benzooxazine (3a). A solution of **1** (291 μL, 1.8 mmol) and 2-chloromethyl-4-nitrophenol (162 mg, 0.9 mmol) in MeCN (5 mL) was stirred for 50 min at ambient temperature under N_2. Then, the mixture was stored in a refrigerator for 12 h. The resulting precipitate was filtered and dissolved in H_2O (40 mL). After the addition of aqueous KOH (0.05 M, 5 mL), the solution was extracted with Et_2O (3 × 20 mL). The organic layer was dried ($MgSO_4$) and filtered, and the solvent was distilled off under reduced pressure to give **3a** (94 mg, 0.3 mmol) as a white solid. The mother liquor of the initial filtration was concentrated under reduced pressure, and the residue was purified by column chromatography [SiO_2/CH_2Cl_2 → CH_2Cl_2/$MeCO_2Et$ (10:1)] to afford an additional amount of **3a** (60 mg, 0.2 mmol). The overall yield of **3a** was 58%. HPLC [analytical, MeCN/H_2O (80:20)]: RT = 4.5 min, PA = 1.6, APP = 236.7 ± 1.0 nm; mp = 180 °C; FABMS: *m/z* = 311 $[M + H]^+$; ^{1}H NMR (500 MHz, $CDCl_3$): δ 1.17 (3H, s), 1.52 (3H, s), 1.57 (3H, s), 4.60 (2H, s), 6.56 (1H, d, 8 Hz), 6.69 (1H, d, 9 Hz), 6.82 (1H, t, 8 Hz), 7.07 (1H, t, 8 Hz), 7.11 (1H, d, 8 Hz), 7.92 (1H, dd, 3 and 9 Hz), 8.06 (1H, d, 3 Hz); ^{13}C NMR (75 MHz, $CDCl_3$): δ 16.6, 18.9, 26.0, 40.0, 48.0, 102.8, 108.4, 118.2, 118.8, 120.5, 122.3, 123.3, 124.0, 127.6, 138.0, 140.4, 146.6, 159.1.

2-Nitro-5a-phenyl-6,6-dimethyl-5a,6-dihydro-12*H*-indolo[2,1-b][1,3]benzooxazine (4a). A solution of **2** (700 mg, 3.2 mmol) and 2-chloromethyl-4-nitro-phenol (709 mg, 3.8 mmol) in MeCN (30 mL) was heated under reflux for 48 h. After cooling to ambient temperature, the solvent was distilled off under reduced pressure and the residue was dissolved in CH_2Cl_2 (30 mL). The resulting solution was washed with aqueous KOH (0.2 M, 15 mL) and H_2O (15 mL). The organic phase was concentrated under reduced pressure, and the residue was purified by column chromatography [SiO_2/hexane → CH_2Cl_2/hexane (1:1 v/v)] to give **4a** (680 mg, 58%) as a white solid. HPLC [analytical, MeCN/H_2O (95:5)]: RT = 3.6 min, PA = 2.1, APP = 261.0 ± 0.1 nm; mp = 176 °C; FABMS: *m/z* = 372 $[M]^+$; ^{1}H NMR (400 MHz, $CDCl_3$): δ 0.89 (3H, s), 1.60 (3H, s), 4.53 (1H, d, 11 Hz), 4.63 (1H, d, 11 Hz), 6.73 (1H, d, 8 Hz), 6.86−6.94 (2H, m), 7.16−7.19 (2H, m), 7.38−7.42 (3H, m), 7.54−7.65 (2H, m), 7.92−7.94 (2H, m); ^{13}C NMR (100 MHz, $CDCl_3$): δ 18.6, 27.9, 41.0, 49.9, 105.5, 109.2, 118.3, 120.3, 121.0, 122.6, 123.3, 123.9, 127.9, 128.2, 128.8, 129.1, 136.1, 137.9, 141.4, 147.0, 159.3.

X-ray Crystallography. Single crystals of **3a** were grown by vapor diffusion of *i*-Pr_2O/hexane into a MeCN solution of the oxazine. Single crystals of **4c** were grown by vapor diffusion of *i*-Pr_2O into an equimolar MeCN solution of **4a** and Bu_4NOH.

Crystal Data for 3a: $C_{18}H_{18}N_2O_3$, M = 310.34, monoclinic, $P2_1/n$ (no. 14), a = 8.1728(5), b = 17.7129(9), c = 11.0657(6) Å, β = 101.171(5)°, V = 1571.56(15) Å^3, Z = 4, D_c = 1.312 g cm^{-3}, μ(Cu Kα) = 0.735 mm^{-1}, T = 173 K, colorless blocks; 2981 independent measured reflections, F^2 refinement, R_1 = 0.042, wR_2 = 0.113, 2718 independent observed absorption-corrected reflections [$|F_o| > 4\sigma(|F_o|)$, $2\theta_{max}$ = 142°], 209 parameters. CCDC 272868.

Crystal Data for 4c: $(C_{16}H_{36}N)(C_{23}H_{21}N_2O_4)\cdot 2H_2O$, M = 667.91, monoclinic, $C2/c$ (no. 15), a = 37.174(2), b = 9.2670(7), c = 22.8271(17) Å, β = 103.270(6)°, V = 7653.9(9) Å^3, Z = 8, D_c = 1.159 g cm^{-3}, μ(Cu Kα) = 0.616 mm^{-1}, T = 173 K, yellow blocks; 7252 independent measured reflections, F^2 refinement, R_1 = 0.064, wR_2 = 0.183, 5291 independent observed absorption-corrected reflections [$|F_o| > 4\sigma(|F_o|)$, $2\theta_{max}$ = 143°], 538 parameters. CCDC 272869.

Molecular Modeling. The structure of **3a** was built with GaussView[28] and optimized (AM1) with Gaussian.[29] In the resulting geometry, the length of the C−O bond at the junction of the indoline and benzooxazine fragments is 1.469 Å. This value was increased in 10 consecutive steps of 0.1604 Å each. After each increment, the C−O distance was constrained and the overall geometry was re-optimized (AM1). The profile of the minimized energy for the C−O distance drive is illustrated in Figure S6. The structures (**3a** and **3b** in Figure S6) corresponding to the two energy minima were re-optimized [B3LYP/6-31G(d)] with no distance constrains. Frequency calculations [B3LYP/6-31G(d)] on the resulting geometries did not reveal imaginary frequencies, confirming that they correspond to minima on the potential energy surface. The transition state for the transformation of **3a** into **3b** was identified with the QST3 protocol (AM1), using the geometry corresponding to the energy maximum in Figure S6 in conjunction with the corresponding reactant and product. The resulting structures were then optimized [B3LYP/6-31G(d)] using the TS option within Gaussian. Frequency calculations [B3LYP/6-31G(d)] on the final geometry revealed a single imaginary frequency, confirming that it corresponds to a transition state on the potential energy surface. The energies of the three stationary points were corrected to account for the corresponding zero-point energies, using a scaling factor[30] of 1.0119, and are reported in Figure 7.

Steady-State Absorption Spectroscopy. The absorption spectra were recorded either in aerated MeCN, using quartz cells with a path length of 0.5 cm, or in PMMA matrixes. The polymer films were prepared by spin-coating aliquots of CH_2Cl_2 solutions of PMMA (160 mg mL^{-1}) and either **3a** or **4a** (8 mg mL^{-1}) with and without Bu_4NOH (7 equiv) on glass plates at 420 rpm for 9 s. The thicknesses of the resulting films were ca. 6 μm and were measured with a digital micrometer.

Transient Absorption Spectroscopy. The absorption spectra were recorded with a commercial laser flash photolysis apparatus either in aerated MeCN, using quartz cells with a path length of 1.0 cm, or in PMMA matrixes. The excitation source was a Nd:YAG laser (355 nm, 6 ns, 8 or 12 mJ). The quantum yield (Φ) for the photoinduced ring opening of **3a** and **4a** was determined with eq 1, using an optically matched MeCN solution of benzophenone as standard. The quantum yield (Φ_{BE}) for the intersystem crossing of benzophenone is unity, and the molar extinction coefficient (ϵ_{BE}) for its triplet absorption at 520 nm is 6.5 mM^{-1} cm^{-1}.[31] The molar extinction coefficient (ϵ) of the ring-opened isomers at 440 nm was estimated to be ca. 22 mM^{-1} cm^{-1} from the absorption spectrum of **8** (e in Figure 8). The terms χ and χ_{BE} in eq 4 are the slopes of the linear portions of plots of the photoinduced absorbance changes, measured at the end of the pulse, for the ring-opened isomer and the benzophenone triplet, respectively, against the energy of the laser pulse.

$$\Phi = \frac{\chi \epsilon_{BE} \Phi_{BE}}{\chi_{BE} \epsilon} \qquad (4)$$

(28) GaussView 2.1; Gaussian, Inc.: Pittsburgh, PA, 1998.

(29) Frisch, M. J.; Trucks, G. W.; Schlegel, H. B.; Scuseria, G. E.; Robb, M. A.; Cheeseman, J. R.; Zakrzewski, V. G.; Montgomery, J. A., Jr.; Stratmann, R. E.; Burant, J. C.; Dapprich, S.; Millam, J. M.; Daniels, A. D.; Kudin, K. N.; Strain, M. C.; Farkas, O.; Tomasi, J.; Barone, V.; Cossi, M.; Cammi, R.; Mennucci, B.; Pomelli, C.; Adamo, C.; Clifford, S.; Ochterski, J.; Petersson, G. A.; Ayala, P. Y.; Cui, Q.; Morokuma, K.; Malick, D. K.; Rabuck, A. D.; Raghavachari, K.; Foresman, J. B.; Cioslowski, J.; Ortiz, J. V.; Baboul, A. G.; Stefanov, B. B.; Liu, G.; Liashenko, A.; Piskorz, P.; Komaromi, I.; Gomperts, R.; Martin, R. L.; Fox, D. J.; Keith, T.; Al-Laham, M. A.; Peng, C. Y.; Nanayakkara, A.; Gonzalez, C.; Challacombe, M.; Gill, P. M. W.; Johnson, B.; Chen, W.; Wong, M. W.; Andres, J. L.; Gonzalez, C.; Head-Gordon, M.; Replogle, E. S.; Pople, J. A. *Gaussian 98*, revision A.7; Gaussian, Inc.: Pittsburgh, PA, 1998.

The evolution of singlet oxygen ($^1\Delta_g$) in the course of the photoinduced ring opening of **4a** was monitored by luminescence measurements in air-saturated MeCN. Upon laser excitation of **4a**, the emission of singlet oxygen at 1.27 μm was probed orthogonally to the exciting beam with a preamplified (low impedance) Ge photodiode (300-ns resolution) maintained at 77 K and coupled to a long-pass silicon filter (>1.1 μm) and an interference filter (1.27 μm). The temporal profile of the luminescence was fitted to a monoexponential decay function with the exclusion of the initial portion of the plot, which is affected by the scattered excitation. The luminescence at initial time was extrapolated from the curve fitting. The quantum yield ($\Phi_{\Delta 1}$) of singlet oxygen was determined with eq 5, using an optically matched and air-saturated MeCN solution of benzophenone as standard. The quantum yield ($\Phi_{\Delta 2}$) of singlet oxygen formed upon excitation of benzophenone is 0.37.[32] The terms χ_1 and χ_2 in eq 2 are the slopes of the linear portions of plots of the singlet-oxygen luminescence, determined at initial time upon excitation of **4a** and benzophenone, respectively, against the energy of the laser pulse.

$$\Phi_{\Delta 1} = \frac{\chi_1 \Phi_{\Delta 2}}{\chi_2} \tag{5}$$

Acknowledgment. We thank the National Science Foundation (CAREER Award CHE-0237578), University of Miami, and MIUR (Rome, Italy) for financial support.

Supporting Information Available: General methods and experimental procedure for the synthesis of **2** and **6**, partial ^{1}H NMR spectra of **4a** at various temperatures, partial ^{1}H NMR spectra of **3a** before and after the addition of Bu_4NOH, single-crystal X-ray structures (ORTEP) of **3a** and **4c**, ground-state potential energy profile (AM1) of **3a**, computational data (B3LYP) for **3a**, **3b**, and the transition state, steady-state absorption spectra of **4a** before and after the addition of Bu_4NOH, transient absorption spectra of **3a**, and kinetic trace for the photoisomerization of **4a**. This material is available free of charge via the Internet at http://pubs.acs.org.

JO051417W

(30) Foresman, J. B.; Frisch, Æ. *Exploring Chemistry with Electronic Structure Methods*; Gaussian, Inc.: Pittsburgh, PA, 1996.
(31) Bensasson, R. V.; Gramain, J. C. *J. Chem. Soc., Faraday Trans.* **1980**, *76*, 1801−1810.
(32) Wilkinson, F.; Helman, W. P.; Ross, A. B. *J. Phys. Chem. Ref. Data* **1993**, *22*, 113−262.